JOURNAL OF GEOPHYSICAL RESEARCH, VOL. 115, A00I13, doi:10.1029/2010JA015748, 2010

Comprehensive ground-based and in situ observations of substorm expansion phase onset

A. P. Walsh,[1] I. J. Rae,[2] A. N. Fazakerley,[1] K. R. Murphy,[2] I. R. Mann,[2] C. E. J. Watt,[2] M. Volwerk,[3] C. Forsyth,[1] H. J. Singer,[4] E. F. Donovan,[5] and T. L. Zhang[3]

Received 31 May 2010; revised 10 September 2010; accepted 16 September 2010; published 18 December 2010.

[1] In this paper, we present comprehensive ground-based and space-based in situ geosynchronous observations of a substorm expansion phase onset on 1 October 2005. The Double Star TC-2 and GOES-12 spacecraft were both located within the substorm current wedge during the substorm expansion phase onset, which occurred over the Canadian sector. We find that an onset of ULF waves in space was observed after onset on the ground by extending the AWESOME timing algorithm into space. Furthermore, a population of low-energy field-aligned electrons was detected by the TC-2 PEACE instrument contemporaneous with the ULF waves in space. These electrons appear to be associated with an enhancement of field-aligned Poynting flux into the ionosphere which is large enough to power visible auroral displays. The observations are most consistent with a near-Earth initiation of substorm expansion phase onset, such as the Near-Geosynchronous Onset (NGO) substorm scenario. A lack of data from further downtail, however, means other mechanisms cannot be ruled out.

Citation: Walsh, A. P., et al. (2010), Comprehensive ground-based and in situ observations of substorm expansion phase onset, *J. Geophys. Res.*, *115*, A00I13, doi:10.1029/2010JA015748.

1. Introduction

[2] After almost half a century of study, many different observational characteristics of the substorm process have been identified. Even so, the exact sequence of events surrounding the onset of the substorm expansion phase has not been conclusively determined. High temporal resolution measurements of the aurora and geomagnetic field coupled with in situ spacecraft measurements in the critical locations in the magnetotail are needed to resolve this so-called 2-minute problem [e.g., *Ohtani*, 2004]. NASA's THEMIS (Time History of Events and Macroscale Interactions during Substorms) mission was specifically designed with this in mind [*Sibeck and Angelopoulos*, 2008]; however, combinations of Cluster [*Escoubet et al.*, 2001], Double Star [*Liu et al.*, 2005], geosynchronous spacecraft, IMAGE (Imager for Magnetopause-to-Aurora Global Exploration) [*Gibson et al.*, 2000], and ground-based observations are also well suited to solving the substorm problem.

[3] Regardless of whether the Near Earth Neutral Line [NENL; e.g., *Baker et al.*, 1996], Current Disruption [CD; e.g., *Lui*, 1996] or any other substorm paradigm is considered to be the most accurate macroscale description of events surrounding expansion phase onset, certain physical processes are known to occur during substorms and are still not definitively explained. The disruption of the cross-tail current is certainly important under both the NENL and CD paradigms. Under the NENL framework, the braking of fast flows from their source at a reconnection site ~20–30 R_E downtail from Earth [*Nagai et al.*, 1997] is thought to generate an inertial current in the near-Earth magnetotail. This then disrupts the cross-tail current [*Shiokawa et al.*, 1997] and diverts it along the geomagnetic field into the ionosphere to form the substorm current wedge (SCW), subsequently exciting the aurora. Conversely, in the CD paradigm, a thin current sheet, possibly embedded in a thicker plasma sheet, develops between 10 and 12 R_E downtail during the growth phase of the substorm [*Lui*, 1996]. At some point, this current sheet reaches some critical thickness and becomes unstable, allowing an as-yet-unidentified instability to grow and disrupt the cross-tail current, diverting it along the magnetic field into the ionosphere, forming the SCW and exciting the aurora. Candidate instabilities include the ballooning instability [e.g., *Voronkov et al.*, 1997; *Horton et al.*, 2001; *Saito et al.*, 2008] and cross-field current instabilities [*Lui*, 2004]. Further instability sites subsequently develop along the magnetotail, at one of which reconnection begins, generating fast earthward and tailward flows [*Lui*, 1996].

[4] Common to both these scenarios is the diversion of the cross-tail current into the ionosphere forming the substorm

[1]Mullard Space Science Laboratory, University College London, Dorking, UK.
[2]Department of Physics, University of Alberta, Edmonton, Alberta, Canada.
[3]Space Research Institute, Austrian Academy of Sciences, Graz, Austria.
[4]NOAA, Space Weather Prediction Center, Boulder, Colorado, USA.
[5]Department of Physics and Astronomy, University of Calgary, Calgary, Alberta, Canada.

0148-0227/10/2010JA015748

current wedge [SCW; *McPherron et al.*, 1973]. The cross-tail current in the magnetosphere flows from the dawnward edge of the tail current sheet to the duskward, closing around the magnetopause to make a Θ shape when viewed in the GSM *y*-*z* plane. When this current is disrupted, a portion of the cross-tail current flows into the ionosphere via field-aligned currents (FACs), westward through the ionosphere, and back out of the ionosphere to the magnetotail current sheet via further FACs. It is this upward-directed field-aligned current (and the associated downward-flowing electrons) in the western part of the SCW that is thought to be responsible for the large-scale substorm aurora, and the azimuthal expansion of the SCW for the westward-traveling surge seen in canonical auroral substorms [*Akasofu*, 1964].

[5] Ultra-low-frequency (ULF) magnetic waves are an integral part of the substorm process and have been associated in the literature with auroral activity since the 1800s [*Stewart*, 1861]. Pi2 pulsations, with periods between 40 and 150 seconds [*Jacobs et al.*, 1964], have long been associated with substorm onset and the formation of the SCW [*Olson*, 1999, and references therein]. Pi2 ULF waves can be compressional or shear-mode Alfvén waves and have been detected in association with flow channels in the magnetotail plasma sheet [*Volwerk et al.*, 2005]. They are thought to be directly driven by BBFs at times [*Kepko and Kivelson*, 1999], or they may simply have a source common to that of BBFs (K. Murphy et al., The dependence of Pi2 waveforms on periodic velocity enhancements within bursty bulk flows, submitted to *Annales Geophysicae*, 2010). Shorter-period Pi1 pulsations (1–40 s), which can be further subcategorized into impulsive Pi1Bs and more continuous Pi1Cs [*Heacock*, 1967], have also been studied in the context of substorms [*Arnoldy et al.*, 1998; *Lessard et al.*, 2006]. Unlike Pi2s, which respond globally to substorm onset to the extent that they are observed close to the dip equator [*Olson*, 1999; *Yumoto et al.*, 2001], the Pi1B response in the ionosphere was thought to be more confined to the locality of substorm onset [*Bösinger and Yahnin*, 1987]; however, recent statistical work [*Murphy et al.*, 2010; *Rae et al.*, 2010b] has shown that in fact the ULF spectrum at onset is well described by a power law, and Pi1s and Pi2s decay at the same rate in both latitude and longitude. Pi1s appear more localized because of their smaller amplitude, which means they reach the noise floor of magnetometers more quickly than Pi2s. In the magnetosphere, Pi1B pulsations are thought to be related to the dipolarization of the magnetic field at geosynchronous orbit around substorm onset [*Arnoldy et al.*, 1998; *Lessard et al.*, 2006]. More recently, long-period Pi1s and short-period Pi2s (hereafter termed Pi1-2) ULF waves have been used in timing and localizing substorm onset in the ionosphere [*Milling et al.*, 2008; *Murphy et al.*, 2009a; *Rae et al.*, 2009a, 2009b]. This ULF band has been observed to occur prior to auroral breakup [*Murphy et al.*, 2009a, 2009b] and conjugate in time and space with the formation of wavelike fluctuations along the substorm onset arc seen prior to dipolarization in the magnetosphere [*Rae et al.*, 2009a, 2009b, 2010a].

[6] Here we concentrate on the near-Earth features of substorm onset, namely, the disruption of the cross-tail current and formation of the substorm current wedge using detailed in situ spacecraft data from within the substorm current wedge, and conjugate auroral and ground magnetic observations.

2. Observations

[7] The interval of interest began at 0330 UT on 1 October 2005 and lasted for 2 hours. During the interval Double Star TC-2 [*Liu et al.*, 2005] was inbound toward perigee and located in the premidnight geosynchronous region, duskward of GOES-12. Both spacecraft were located in the Northern Hemisphere. At 0420 UT, the magnetic foot point of TC-2, as calculated using the magnetic field model of *Tsyganenko and Stern* [1996, henceforth T96], was located just east of the Churchill Line of CARISMA (Canadian Array for Realtime Investigations of Magnetic Activity) [*Mann et al.*, 2008] magnetometers in eastern Canada, at a latitude between those of Gillam (GILL) and Island Lake (ISLL). The foot point of GOES-12 was located east of TC-2, just south of Poste de-la-Baleine (PBQ). These spacecraft foot points, along with the locations of relevant ground observation sites, are plotted in Figure 1, as are the orbits of TC-2 and GOES-12 during the interval of interest. All T96 calculations made throughout this paper were based on 1-minute resolution 1 AU OMNI data downloaded from the CDAWeb and hourly *Dst* values.

[8] During this interval, the IMAGE spacecraft was observing the southern polar region. The Frey substorm onset list [*Frey and Mende*, 2006], which was collated through automated examination of the data returned by the FUV instrument [*Mende et al.*, 2000a], recorded the time of global auroral intensification of a substorm onset beginning at 0421 UT. Note that because of the 2-minute cadence of the FUV imagers, this global auroral intensification could have occurred at any time between 0419 UT and 0421 UT. Selected global auroral images taken by the WIC camera [*Mende et al.*, 2000b], part of the FUV instrument, during the interval of interest are plotted in Figure 2. The image representing substorm onset as defined in the Frey list (henceforth referred to as the Frey onset) is labeled in red. Before the Frey onset, the auroral oval was in a quiescent state with no localized sites of activity. The Frey onset, occurring between 0419:15 UT and 0421:21 UT, was a localized site of brighter aurora which remained roughly constant in size, luminosity, and location over the next four auroral images. A further auroral brightening located a few degrees east of the Frey onset, closer to midnight MLT, which became apparent between 0421:20 UT and 0423:26 UT, went on to expand poleward and westward in the manner of a canonical auroral substorm [*Akasofu*, 1964]. Given the spatial and temporal resolution of IMAGE, it is difficult to determine whether the Frey onset and the subsequent activation are actually distinct auroral forms or whether the subsequent activation is simply an expansion of the aurora associated with the Frey onset. Between 0444:18 UT and 0446:23 UT, a further activation along the poleward edge of the now expanded auroral substorm bulge, was observed between ~2100 MLT and ~2400 MLT. This activation was of greater luminosity than the aurora associated with the onset of the auroral substorm and lasted until ~0505 UT. In summary, it is more likely that the auroral brightening at 0421:20–0423:26 UT represented the substorm onset and that the prior intensification represented an initial brightening.

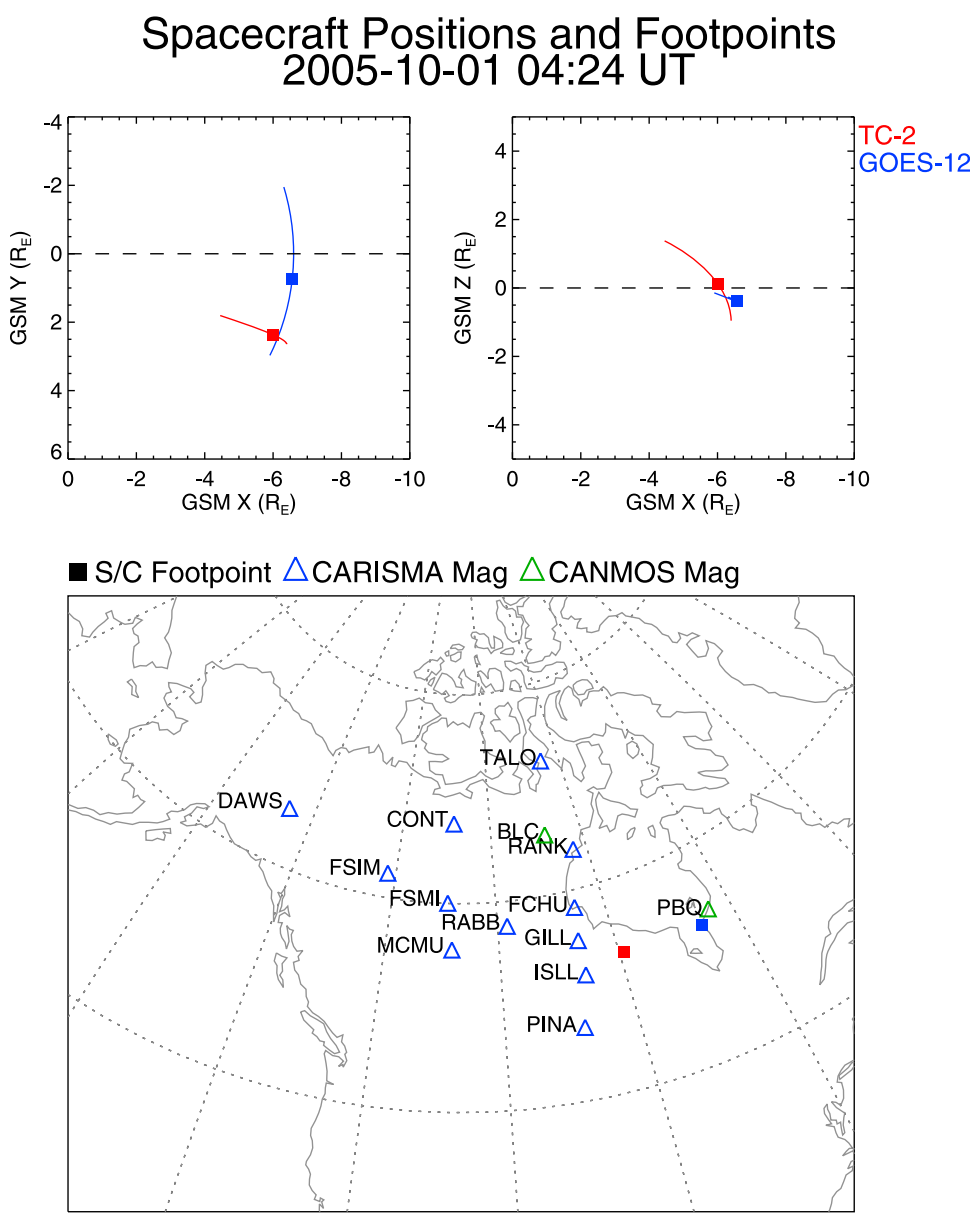

Figure 1. The GSM locations and orbit tracks of both Double Star TC-2 (red) and GOES-12 (blue) in the GSM *x*-*y* and *x*-*z* planes (top) along with the respective T96 foot points of the spacecraft and the locations of various CARISMA and CANMOS magnetometer sites (bottom).

[9] Determining the exact conjugate location of auroral substorm onset in the Northern Hemisphere is difficult without Northern Hemisphere global auroral images, particularly for this event, where there was no extended period of southward IMF (data not shown), precluding the application of the empirical formula of *Østgaard et al.* [2004]. Fortunately, this particular substorm happened in the Canadian sector, so a variety of ground-based instrumentation can be used to study the onset in the Northern Hemisphere in the absence of global auroral imaging.

2.1. Ionospheric Signatures of the Substorm

[10] The Geodetic *x* (i.e., northward) component of the geomagnetic field as measured by various CARISMA magnetometer stations that make up part of the Churchill Line (the locations of which are marked on Figure 1) is plotted in Figure 3, along with auroral data in the 558 nm band from the NORSTAR or Northern Solar Terrestrial Array (formerly CANOPUS, or Canadian Auroral Network for the OPEN Program Unified Study) Meridian Scanning Photometer [MSP; *Rostoker et al.*, 1995; *Donovan et al.*, 2003] located at GILL. Note that the magnetometer traces are individually scaled. Large negative geomagnetic bays can be seen in the traces from several magnetometer stations, at GILL starting at ~0420 UT (red dashed line) and FCHU at ~0425 UT. Further negative bays were detected beginning at ~0445 UT at higher-latitude stations, notably RANK, where a change in the magnetic field of ~900 nT was detected, more than twice that detected by any of the other CARISMA magnetometer stations. The 558 nm (green line) auroral data show a brightening of the aurora at GILL after the 0420 UT data gap (the periodic gaps in the MSP data are the result of an

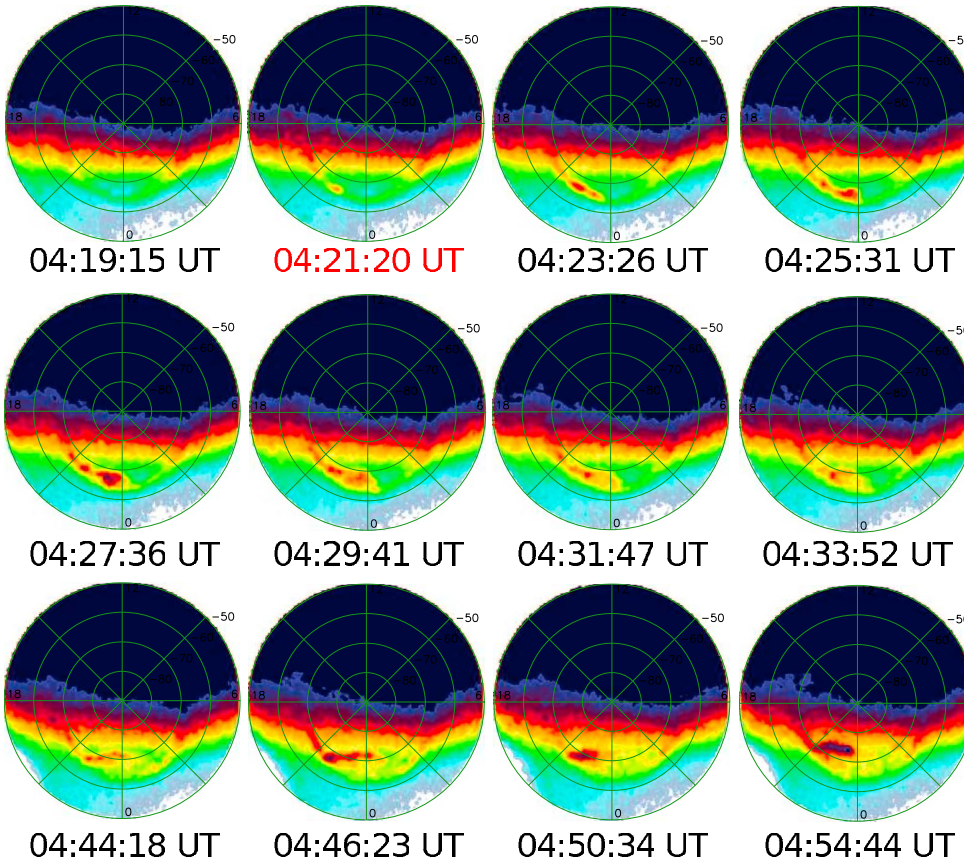

Figure 2. Data from FUV-WIC onboard the IMAGE spacecraft. Substorm onset from the list of *Frey and Mende* [2006] is labeled in red.

instrument electronics glitch). Raw data from the Multispectral All Sky Imager at the same observation site (not shown here) time the auroral brightening at 0420 UT. This auroral brightening presumably represents the conjugate aurora to those seen in the 0419:15 UT–0421:21 UT WIC frame (the Frey onset).

[11] The Automated Wavelet Estimation of Substorm Onset and Magnetic Events [AWESOME; *Milling et al.*, 2008; *Murphy et al.*, 2009a] technique utilizes a discrete wavelet transform with a Meyer wavelet basis to determine the onset time and characteristics of ULF waves as a function of frequency observed by magnetometers. Through the calculation of a quiet time noise threshold for each frequency, AWESOME is able to specify an onset time as the time at which a continuous series of wavelet coefficients rises above the predetermined noise threshold. Combining the AWESOME ULF onset times from numerous magnetometer stations enables the location of ULF onset in space as well as time to be determined. Figure 4, bottom, is an AWESOME wavelet spectrogram calculated for the GILL magnetometer. The x-axis represents time in seconds from 0412 UT and the y-axis denotes ULF wave period. The right-hand y-axis labels are the onset times in each wave band, and the color scale represents normalized wave power. A clear onset of ULF waves is observed at 0416:00 ± 16 s UT in the 24–96 s Pi1-2 wave band, followed by an intensification at 0423 UT. The top left plot shows the Frey onset WIC image (0419:15 UT–0421:20 UT) mapped to the Northern Hemisphere by simply reversing the magnetic latitude. Overplotted on the WIC image is a minimum curvature fit to the ULF wave onset time derived from AWESOME analyses of data from the marked magnetometer stations, relative to auroral onset. The initial onset was located close to GILL and first detected at 0416:00 UT ± 16 s, i.e., 3–5 minutes prior to global auroral onset. The ULF onset begins at the same location as that determined from the ground-based optical data, while the IMAGE onset was located slightly east of this, presumably due to mapping errors. The top right is the equivalent plot for the ULF intensification that was first detected at ISLL at 0422:24 UT (see Figure 7 for a wavelet spectrogram of this intensification) overplotted on the 0421:20 UT–0423:26 UT IMAGE (i.e., the frame following the Frey onset frame). The ULF intensification was located south of ISLL and PBQ but cannot be further localized using AWESOME because of the lack of spatial coverage of magnetometer stations in that region. Note that amplitude-time traces of the Pi1-2 wavelet from GILL and ISLL are plotted in Figures 7a and 7b. Data from the CPMN [*Yumoto et al.*, 2001] low-latitude magnetometer stations at Ancon and Guadalupe, Peru, which are located near the dipole equator and the orbit track of GOES12 (not shown), suggest a low-latitude Pi2 onset around 0420 UT, consistent with

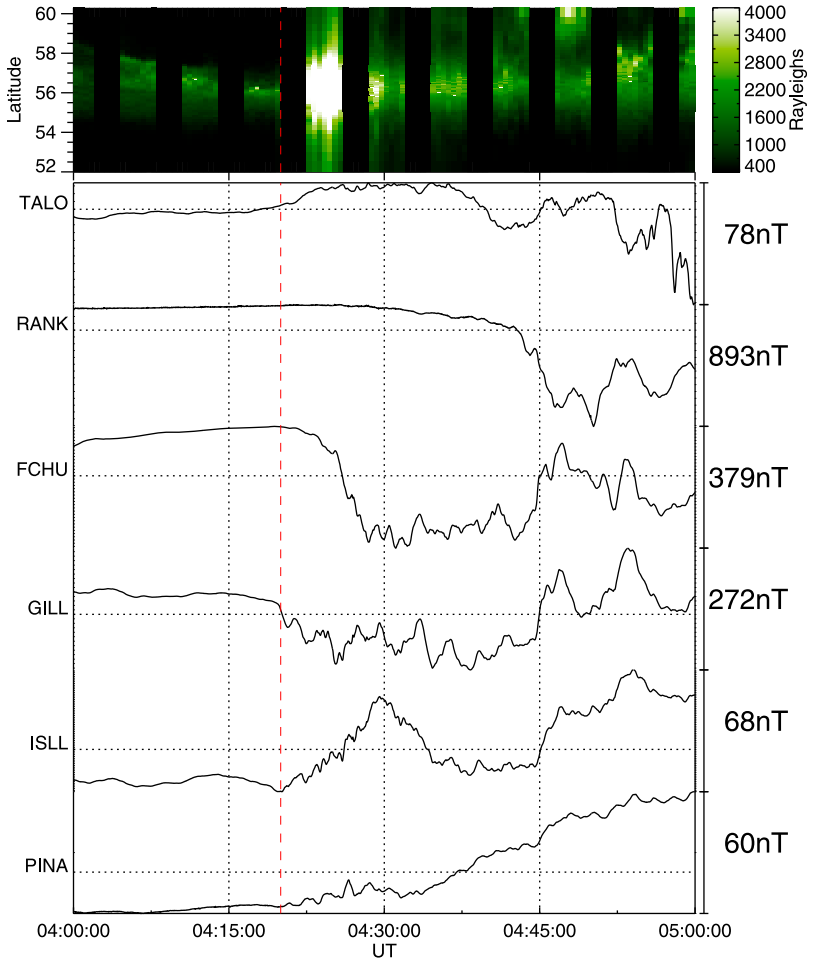

Figure 3. The *x*-component of the geomagnetic field as measured at several Churchill line CARISMA magnetometers (bottom) and a keogram green line (i.e., 558 nm) emission measured by the meridian scanning photometer at GILL (top). Periodic data gaps in the photometer data are a result of an instrument electronics glitch.

the auroral onsets seen by IMAGE and the ground-based optics.

2.2. Near-Earth Magnetosphere Signatures of the Substorm

[12] The TC-2 and GOES 12 spacecraft, separated by ~1.8 R_E (mostly in GSM *y*) and with their T96 foot points located between the GILL, ISLL, and PBQ observation sites were ideally located to observe the effects of the substorm at geosynchronous orbit. Data from the GOES-12 magnetometer [*Singer et al.*, 1996] and the FGM [FluxGate Magnetometer; *Carr et al.*, 2005] magnetic field and PEACE [Plasma Electron And Current Experiment; *Fazakerley et al.*, 2005] electron instruments onboard TC-2 are plotted in Figure 5, where Figure 5a contains the magnitude and GSM components of magnetic field from TC-2 (all spacecraft data throughout this paper are in GSM coordinates unless otherwise specified). Figures 5b–5d are the components of magnetic field from TC-2 (red) and GOES-12 (black) with a T96 model field subtracted (referred to as dB_x, dB_y, and dB_z, respectively). Figure 5e contains the PEACE electron number density, and Figure 5f shows the *x*-component of the electron velocity perpendicular to the magnetic field, as projected onto GSM axes. Figure 5g is the ratio of the parallel and perpendicular electron temperatures ($T_{e\|}/T_{e\perp}$). The velocity data have been smoothed over five data points, while the temperature ratio and density are unsmoothed. Figures 5h–5j are energy-time spectrograms plotting differential energy flux of electrons with pitch angles of 0°, 90°, and 180°, respectively.

[13] Both GOES-12 and TC-2 measure a stretching of the geosynchronous magnetic field (i.e., an increase in dB_x) beginning at ~0404 UT (Figure 5b) and lasting until ~0420 UT, when both spacecraft saw significant changes in the magnetic field. Wave activity became obvious in time series of the dB_x and dB_z (Figures 5b and 5d) components of the magnetic field, while TC-2 recorded a negative deviation in dB_y and GOES-12 recorded a positive deviation in dB_y (Figure 5c). These deviations lasted until ~0425 UT, when the field on both spacecraft returned to a value close to the predicted model field. Immediately afterward, further deviations in dB_y of the same sense as before were observed, along with a negative (positive) deviation of dB_x on GOES-12 (TC-2). At ~0426 UT, GOES-12 observed a sharp dipolarization, while TC-2 observed a slower, more smooth dipolarization beginning at ~0428 UT and lasting for approximately 10 minutes, by which time dB_z had reached the

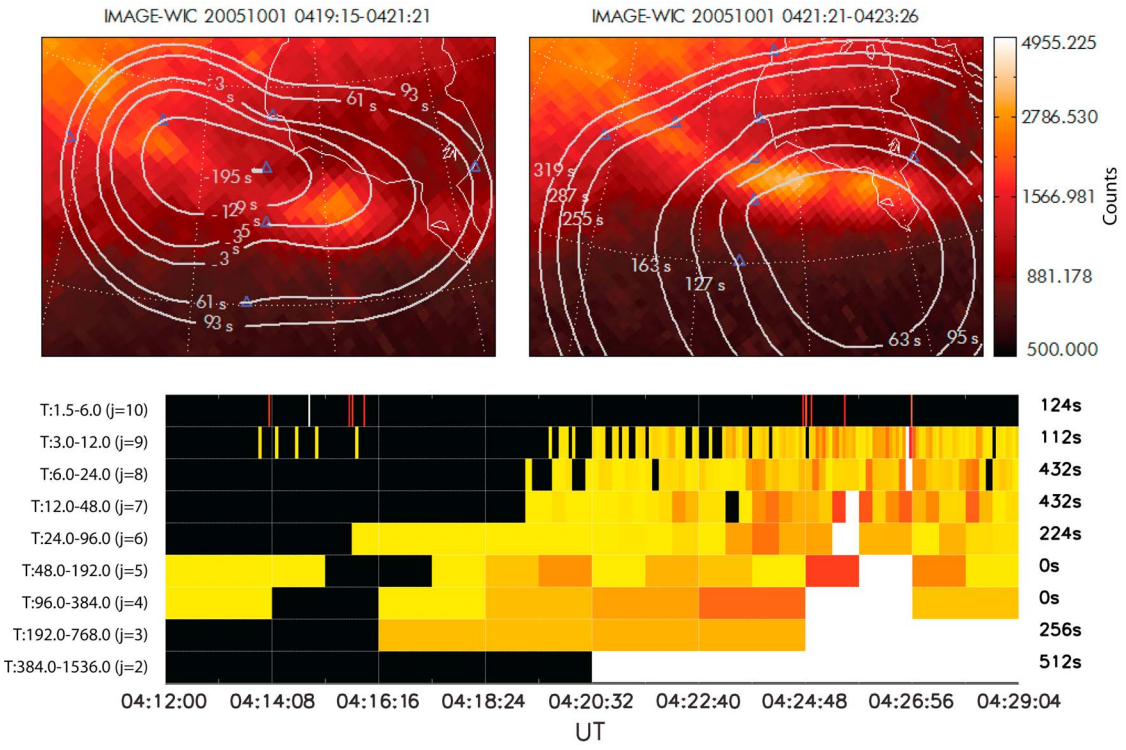

Figure 4. The bottom is an AWESOME wavelet spectrogram for the GILL magnetometer. The *x*-axis represents seconds from 0412 UT, the *y*-axis different wavelets. Numbers on the right-hand side are the time at which significant ULF power was first detected in that wavelet. The color scale represents normalized wave power. The top two parts are minimum curvature fits to the AWESOME data for several magnetometers (GILL onset is on the left, the subsequent ISLL intensification is on the right) overplotted on IMAGE FUV data.

same level as on GOES-12 and dB_y on both spacecraft had returned to zero.

[14] Unfortunately, there is a data gap in the TC-2 PEACE data between 0415 UT and 0423 UT caused by a commanded instrument reset, so any link between the characteristics of the electron distributions and the wave activity cannot be unambiguously determined; however, the electron data still show several interesting features during this interval. Before the period of activity, PEACE measured electron distributions that were dominated by field-perpendicular particles, as expected for the near-Earth plasma sheet (Figures 5g–5j). At the end of the data gap (~0424 UT), this distribution had changed significantly. Much higher fluxes of electrons were measured, and a population of lower-energy, field-aligned electrons are evident in the 0° (i.e., into the northern ionosphere) and 180° (out of the northern ionosphere) pitch angle spectrograms (Figures 5h and 5j) between ~100 eV and ~1000 eV. This population was present until the dipolarization started at ~0428 UT and can also be seen as a change in $T_{e\|}/T_{e\perp}$ such that it rises above 1. No significant plasma flow was observed before the start of the dipolarization, at which time TC-2 PEACE recorded earthward flows (i.e., $v_{\perp x} > 0$) that lasted for the duration of the dipolarization of the magnetic field at TC-2 (Figure 5f).

[15] In addition to the above, the SOPA instrument on the Los Alamos 1990–095 geosynchronous spacecraft [e.g., *Belian et al.*, 1992] detected an energetic particle injection at 0425 UT, which was also seen as an increase in radio absorption by the NORSTAR riometer [e.g., *Spanswick et al.*, 2007] at FCHU. The riometer at GILL detected a smaller injection at 0420 UT (data not shown here).

3. Analysis

[16] Both the ground- and space-based magnetic field data presented above can be interpreted in terms of a substorm current wedge located near the spacecraft and magnetometer stations. *Smith et al.* [2002] described a method whereby the sense of the changes (i.e., positive or negative) in the deflection of the three components of the geomagnetic field detected by magnetometer stations immediately prior to and following substorm onset can be used to estimate the location of the substorm electrojet and the field-aligned currents that make up the substorm current wedge in the ionosphere. In this paper, we use the 5 minutes prior to and following onset, which was defined as the first detection of bright aurora in the ground-based optics (0420UT ± 15 s). *D*- and *z*-components of magnetic field from FCHU, PBQ, and GILL are plotted in Figures 6a–6c, respectively. *D*-components are plotted in green and *z*-components are plotted in blue. Red dashed lines mark the times between which changes in the field components are used to estimate the location of current systems. Figure 6d is a map of various CARISMA and CANMOS magnetometer sites, where each site is marked with the sense of the changes in the *h*-, *d*- and *z*-components of the magnetic field at that magnetometer in red, green, and blue, respec-

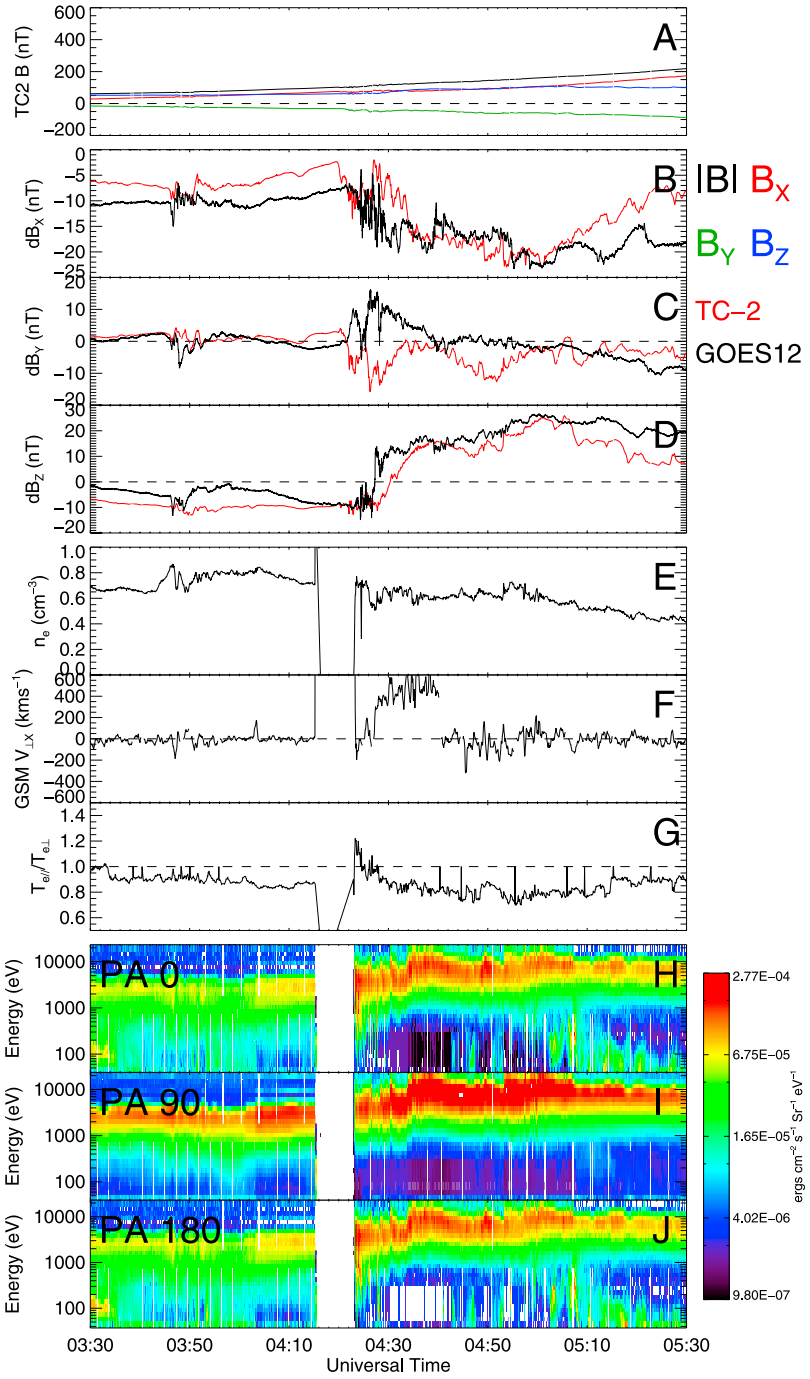

Figure 5. A comparison of the results of AWESOME on the ground and AWESOME:ST in space. (a) Wave power in the Pi1-2 overlap band accompanied by the relevant AWESOME spectrogram. (b) Equivalent for ISLL. (c) The AWESOME:ST results for GOES-12 ($B_{\|}$ black, B_r red) with relevant wavelet spectrograms underneath. (d) The equivalent for TC-2.

tively. The estimated latitude of the westward electrojet (close to GILL) is marked with a horizontal dashed line, while the vertical dashed line marks the estimated central meridian of the SCW, between the Churchill Line and the PBQ magnetometer station. Because of magnetometer coverage, the location of the SCW field-aligned currents is not well defined in this case; however, the upward field-aligned current at the west of the wedge, associated with downward-flowing electrons, is likely to be around GILL, based on the changes in the y- and z-components of the geomagnetic field and consistent with the observations of aurora at GILL and in the Frey onset WIC frame (Figures 3 and 4). Given the location of the T96 foot points of GOES-12 and TC-2, marked on Figure 6a as blue and red squares, respectively, one would expect the spacecraft to be located within the earthward portion of the SCW in space, and indeed the spacecraft magnetometer data are consistent with this.

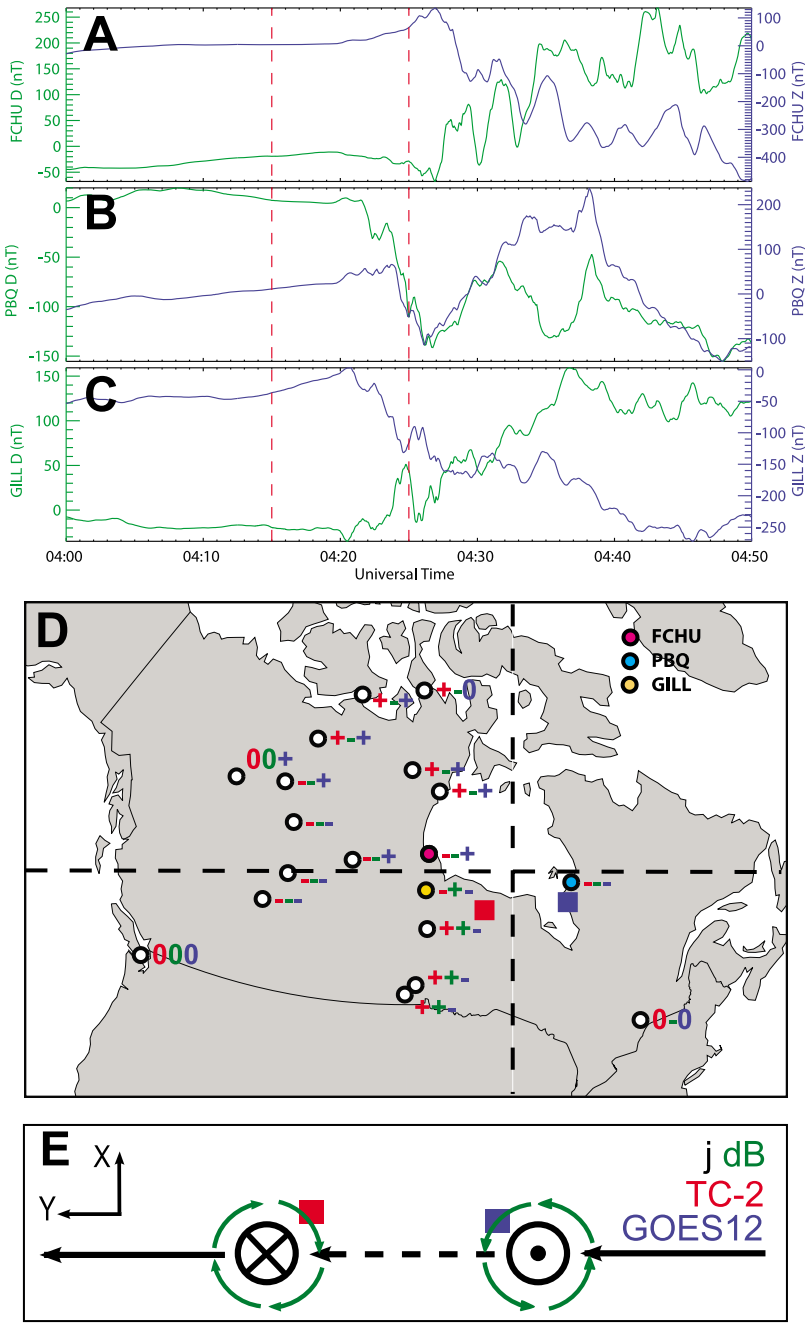

Figure 6. Data from Double Star TC-2 and GOES-12. (a) The magnitude and GSM components of magnetic field from TC-2. (b–d) GSM components of magnetic field from TC-2 (red) and GOES-12 (black) with a T96 model field removed. (e–g) Electron density, $v_{\perp X}$ and $T_{\parallel}/T_{\perp}$, respectively. (h–j) Energy-time spectrograms for electrons with pitch angles of 0°, 90°, and 180°, respectively.

[17] Figure 6e is an illustration of the expected perturbation fields (in GSM coordinates) associated with an SCW in space, with the inferred spacecraft locations relative to the SCW marked again as blue and red squares. The plot is a projection in the GSM x-y plane looking down from the north, so the eastern FAC is flowing out of the page (i.e., into the ionosphere), while the converse is true for the western FAC. The anticorrelated dB_y and, to a lesser extent, dB_x, components of the magnetic field as measured by GOES-12 and TC-2 (Figures 5b and 5c) can be interpreted as the spacecraft being located in the westward (TC-2) and eastward (GOES-12) sectors of the SCW. The later observation of dipolarization (Figure 5d) suggests that both spacecraft were located slightly earthward of the initial reduction in the cross-tail current. That the auroral onset occurred near or over GILL, close to TC-2's foot point, is also consistent with that spacecraft's location being in the western part of the SCW, north of the magnetic equatorial plane. If the spacecraft were in the

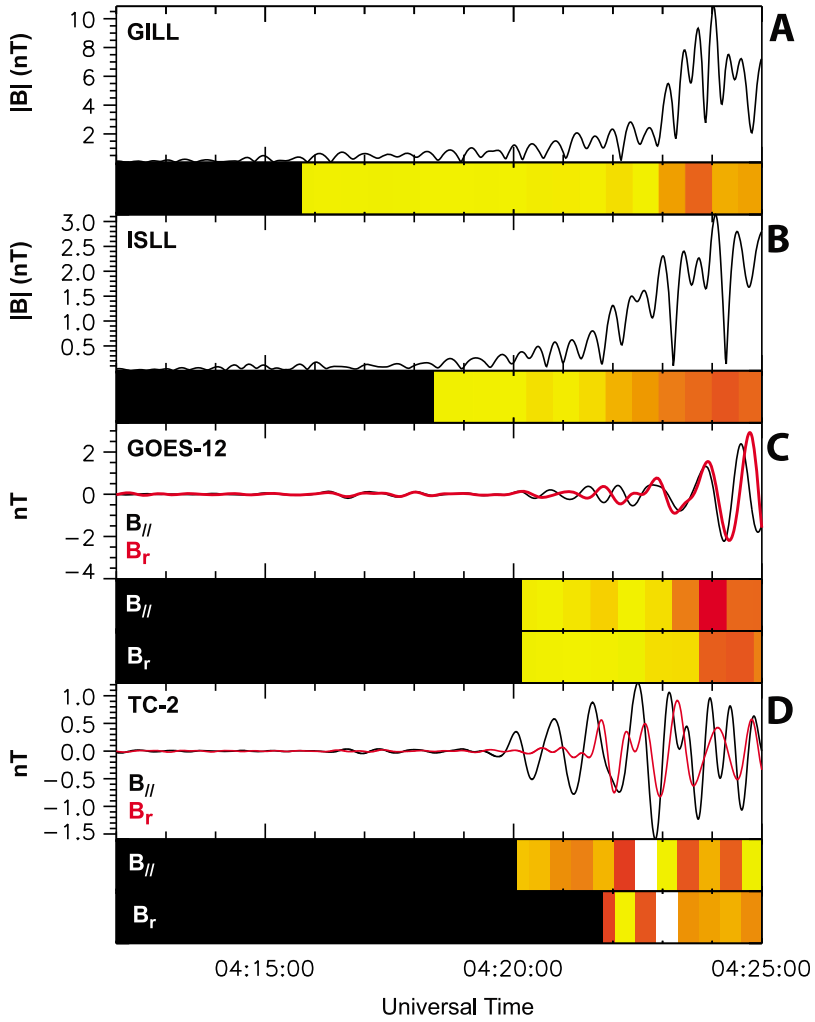

Figure 7. (a–c) *D*-component (green) and *z*-component (blue) of the magnetic field measured by the FCHU, PBQ, and GILL magnetometers, respectively. (a) The estimated location of the substorm electrojet and current wedge FACs based on the method described by *Smith et al.* [2002]. Near the Churchill Line of magnetometers, the electrojet is expected to lie roughly along the black dashed horizontal line, while the vertical line marks the estimated longitude of the central meridian of the SCW. FCHU, PBQ, and GILL are marked by magenta-, cyan-, and yellow-filled circles, respectively. Other magnetometers are marked as white-filled circles. (b) An estimate of TC-2's (red) and GOES-12's (blue) locations with respect to the SCW in space. Figure 7b is the projection of the SCW onto the GSM *x*-*y* plane as viewed from the north.

Southern Hemisphere, the sense of the magnetic perturbations would be opposite.

[18] Given that the locations of the two spacecraft are roughly conjugate to the sites of ULF wave activity determined from AWESOME (Figure 4) within the substorm current wedge (Figures 5 and 6) and that pulsations in the Pi1-2 band were observed in both the GOES and TC-2 magnetometer data, the AWESOME method has been extended to time the onset of waves seen at the spacecraft (Automated Wavelet Estimation of Substorm Onset and Magnetic Events: Spacecraft Timing, AWESOME:ST) so that the Pi1-2 onset times in space and on the ground can be compared. Applying AWESOME to spacecraft data requires a slightly different approach than for ground-based magnetometers. Rather than analyzing the transverse component of the ULF wavefields on the ground, we perform the analysis on individual magnetic field components corresponding to the field-aligned direction, a pseudo-radial direction and a pseudo-azimuthal direction ($B_{||}$, B_r, and B_ϕ, respectively) in a mean field-aligned coordinate system, since we do not presume to know the source of ULF wavefields in space. The mean field-aligned coordinate system was calculated using both a 10-minute boxcar average and a low-pass Fourier filter, which produced comparable results. The coordinate system defined using the Fourier filter was chosen over the boxcar average, since it gave a slightly smoother mean field.

[19] Figure 7 shows a comparison of ground-based and in situ estimates of ULF wave onset in the Pi1-2 ULF wave band. Note that the period bands calculated by the AWESOME algorithm are dependent upon the native temporal resolution of the input time series [see *Murphy et al.*, 2009a, for details]. Hence, the equivalent Pi1-2 overlap bands for the ground magnetometers (1 s temporal resolution; 24–96 s wavelet decomposed Pi1-2 band), GOES magnetic field

(0.512 s temporal resolution; 25–98 s wavelet decomposed Pi1-2 band), TC-2 FGM (22.2 Hz temporal resolution; 19–77 s wavelet decomposed Pi1-2 band) have slightly different period ranges.

[20] Figure 7a (top) shows the wavelet decomposed Pi1-2 power and corresponding (bottom) AWESOME Pi1-2 power spectrogram from the GILL magnetometer. It is clear from the spectrogram in Figure 7a that Pi1-2 power at GILL rises above the noise threshold at 0416:00 UT, as previously discussed, and grows slowly over the subsequent ~7 minutes. Figure 7b shows the equivalent information for the ISLL magnetometer, the location of the first evidence of ULF intensification at 0422:24 UT discussed previously. Evident in Figure 7b is an intensification of ULF wave power at 0422:24 UT, which is closely coincident with the formation of the second auroral activation (see Figures 2 and 4). Note that this intensification is clearer in the wavelet spectrogram as a transition from yellow to orange. Figure 7c shows the results of AWESOME:ST as applied to GOES-12 MFA B in the Pi1-2 overlap band as described above. The red (black) trace corresponds to the radial (parallel) component of B, the AWESOME:ST power spectra of which are shown below the traces, radial above parallel. The first indication of Pi1-2 onset in space above a predetermined noise threshold is at ~0420 UT, some 4 minutes after ground onset of ULF waves but coincident with auroral onset. The noise threshold for AWESOME:ST was defined as the quietest time observed in the 2 hours prior to onset. Note that quiet time activity in both spacecraft magnetometers was much less than that observed on the ground. The delayed detection of ULF wave power at GOES-12 may be a result of the spacecraft not being located in the initial activation region in space. Figure 7d shows the equivalent AWESOME:ST estimate of Pi1-2 onset as observed by TC-2. At TC-2, the $B_{\|}$ component shows a contemporaneous ULF wave onset with GOES-12, but B_r onset is only seen ~2 minutes later. That ULF waves at both TC-2 and GOES 12 began at the same time as auroral onset suggests active M-I coupling was occurring at, or considering the earlier ULF onset at GILL, before, substorm onset near the location of the SCW observed at TC-2 and GOES-12. Indeed, given the small number of spaceborne magnetometers when compared to ground stations employed in this study, it is possible that there was activity in space earlier than 0420 UT, but it was missed by the spacecraft.

[21] The population of lower-energy field-aligned electrons that is responsible for the peak in $T_{e\|}/T_{e\perp}$ (Figures 5f–5i) seen during the wave activity but prior to dipolarization are examined in more detail in Figure 8. The MFA components of magnetic field, measured between 0423 UT and 0425 UT, are plotted in Figure 8a, MFA electric field components (calculated in GSM coordinates as $\mathbf{E} = -\mathbf{v}_e \times \boldsymbol{B}$ using data from PEACE and FGM, before being transformed into the same MFA system as defined for the magnetic field data) are plotted in Figure 8b. Both magnetic and electric field data have been bandpass-filtered in the period range 16–68 s. Note that the nonzero $E_{\|}$ evident in the left-hand side of Figure 8b is a windowing effect of the bandpass filter, present because of the PEACE data gap. Electron differential energy flux for particles with pitch angles of 0°, 90°, and 180° are plotted in Figures 8c, 8d, and 8e, respectively. A spectrogram of the difference between the mean of the field-aligned and anti-field-aligned and the perpendicular electron differential energy flux (i.e., ($PA0$ + $PA180$)/2 − $PA90$) is plotted in Figure 8f, with a color scale such that blue represents perpendicular-dominated electron distributions and red (anti) parallel dominated electron distributions. Similarly, Figure 8g is the difference in differential energy flux between field-aligned electrons and anti-field-aligned electrons, with a color scale such that a net electron energy flux parallel to the magnetic field (i.e., into the northern ionosphere) shows up in red, whereas a net electron energy flux out of the northern ionosphere shows up in blue. From the PEACE data, it can be seen that during this interval, prior to the dipolarization (which began at ~0428 UT), the electron distributions are (anti)parallel dominated, particularly at energies close to and below 1 keV. During and after the dipolarization, the electron distributions become perpendicularly dominated again as the lower-energy field-aligned population disappears. There is a net flux of electrons into the northern ionosphere peaking just before 0424 UT, followed by a slightly lower energy flux of electrons out of the northern ionosphere.

[22] While the PEACE data gap (prior to the interval plotted in Figure 8) precludes making any explicit causal link between the appearance of the field-aligned electron population and the onset of ULF waves at TC-2, as determined by AWESOME:ST, it is possible to examine the characteristics of the ULF waves at the time of the strong net electron energy flux into and then out of the northern ionosphere at 0424 UT. To do so, an estimate of the field-aligned Poynting flux associated with the ULF waves has been made (Figure 8h). Because there is no electric field instrument onboard TC-2, the electric field in the spacecraft frame has been estimated from the PEACE electron velocities and FGM magnetic field data, assuming $\mathrm{E} = -\mathrm{v}_e \times B$, after which both the magnetic and derived electric field data were transformed into MFA coordinates and bandpass-filtered in the period range 16–68 seconds to calculate the Poynting flux in the Pi1-2 overlap band. This passband is slightly smaller than that used for the AWESOME:ST wavelet analysis to ensure that the filter window used in bandpassing the PEACE-derived electric field data does not extend into the data gap when calculating S for the times of greatest field-aligned electron anisotropy; the Poynting flux is therefore likely underestimated. The first vertical line on the plot marks the time at which the PEACE data became usable after the data gap (the previous distributions are incorrect because the instrument's MCP voltage had not reached operational levels); the second vertical line marks the first time at which Poynting flux was calculated using a 16–68 s passband only includes accurate PEACE data. There is a clear enhancement in the field-aligned Poynting flux into the northern ionosphere in the Pi1-2 overlap band at the time of the net electron energy flux into the northern ionosphere. However, while the TC-2 PEACE sensor may not be well-enough calibrated to confidently quantify the Poynting flux enhancements, as an order of magnitude estimate, the measured Poynting flux mapped to the ionosphere will be $\sim 10^{-3}$ W m^{-2}, which is enough to provide the energy to generate visible auroral displays [e.g., *Stenbaek-Nielsen et al.*, 1998]. The electrons themselves carried a net energy flux equivalent to 0.2×10^{-3} Wm^{-2} at the ionosphere, less than has been previously observed [*Wygant et al.*, 2002; *Chaston et al.*, 2005], so, assuming no further acceleration by parallel electric fields, in this case, the

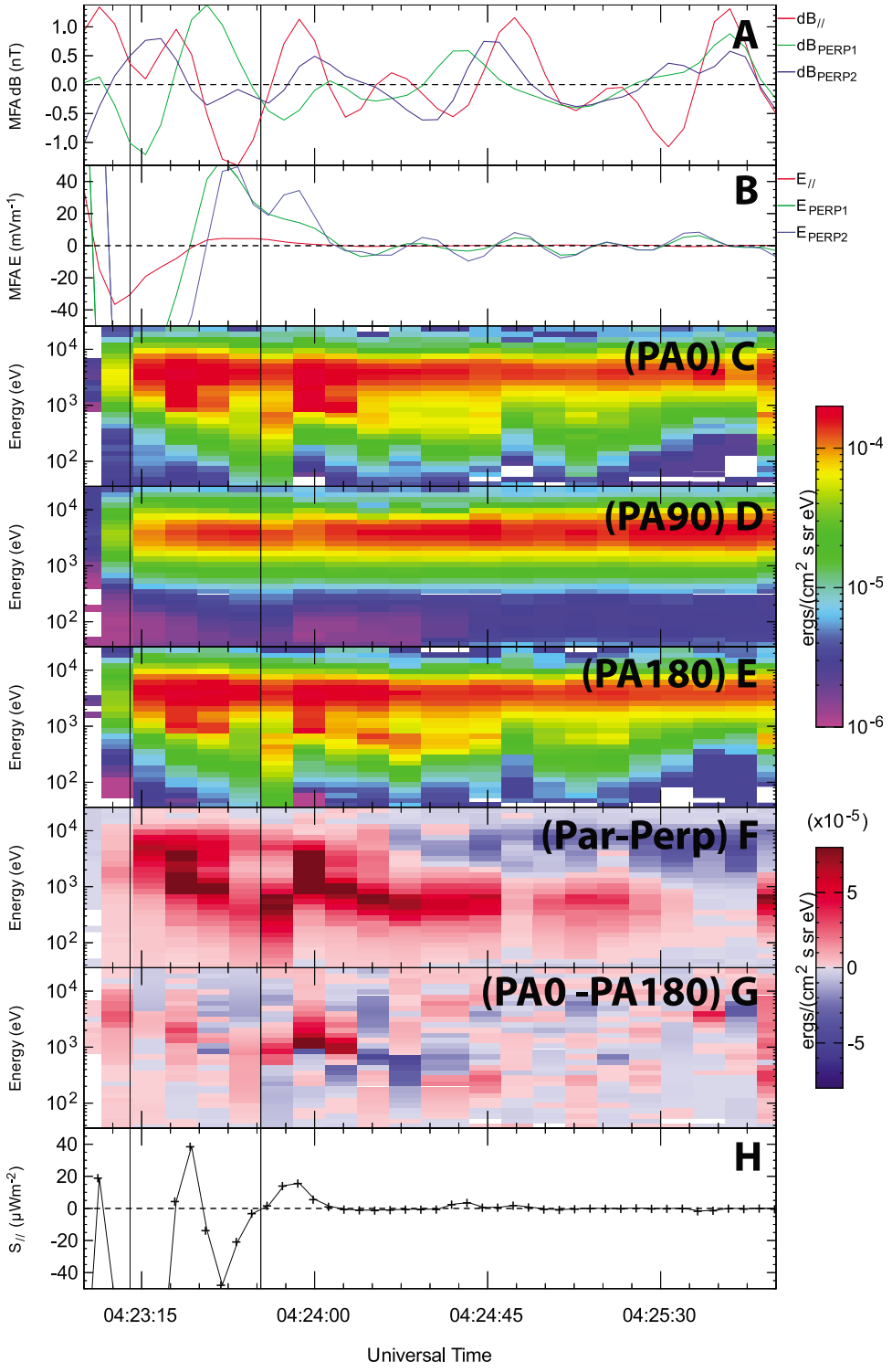

Figure 8. Detailed data from TC-2 taken in the few minutes prior to dipolarization. (a) The MFA components of magnetic field with a T96 model field subtracted. (b) The MFA electric field calculated from $-\mathbf{v_e} \times \mathbf{B}$. (c–e) Electron energy time spectrograms for particles with pitch angles of 0°, 90°, and 180°, respectively. (f) Spectrogram showing the difference between the average of parallel and antiparallel electron energy fluxes and perpendicular energy fluxes, such that a red color represents distributions dominated by (anti) field-aligned electrons and blue represents perpendicular-dominated electron distributions. (g) A similar spectrogram, this time plotting the difference between parallel and antiparallel particles. Red here represents a net electron flux into the northern ionosphere. (h) The field-aligned Poynting flux filtered in the 16–68 s wave band.

waves are providing more of the energy deposited into the ionosphere.

4. Discussion

[23] The evidence presented above suggests that the TC-2 and GOES-12 spacecraft were located within the longitudinal extent of the SCW (starting at 0419 UT) immediately prior to auroral onset over GILL. The dipolarization was only observed several minutes later, which is consistent with the spacecraft being located slightly earthward of the region of current disruption, which later expanded earthward over them, and therefore initially they only detected the magnetic field perturbations associated with the FACs at the western and eastern edges of the SCW. That the spacecraft did not detect any wave or plasma activity at the somewhat earlier onset of ULF activity at GILL, as determined from AWESOME, may be a consequence of their being located at a different longitude from that of the activation region at 0416 UT. This is more convincing in the case of GOES-12, the foot point of which was located further east of GILL closer to PBQ. Indeed, if one tracks the evolution of the ULF onset centred on GILL, the time at which the disturbance is predicted to cross the foot point of GOES-12 is ~0420 UT, the onset time of ULF activity at that spacecraft. TC-2, however, does not fit that pattern, possibly as a result of the combination of nonuniform expansion of the SCW and associated disturbed region in space.

[24] *Murphy et al.* [2009a, 2009b] showed that the ULF onset is routinely observed several minutes before global auroral onset registers in the IMAGE FUV instrument. This is also the case in this event. Recent work by *Milan et al.* [2010] has shown statistically that there is enhanced auroral activity in the location of auroral substorm onset up to an hour prior to that onset. *Rae et al.* [2009a, 2009b] also observed structured, azimuthally expanding, wavelike aurora contemporaneous with ULF onset but prior to global auroral onset. The work of *Murphy et al.* [2009a, 2009b], *Rae et al.* [2009a, 2009b], and *Milan et al.* [2010] is consistent with the idea that there is some sort of preconditioning or precursor activity in the magnetosphere and ionosphere prior to substorm onset, which could be considered in terms of the growth of a region of instability in both the ionosphere and magnetotail, consistent with the delay in observation of ULF onset in space during the event presented above.

[25] The observation of field-aligned Poynting flux enhancements near geosynchronous altitude during substorm times has been made before by, for example, *Maynard et al.* [1996a, 1996b] and *Erickson et al.* [2000]. These authors presented a model whereby the constructive interference of waves carrying field-aligned Poynting flux, caused by the growth of drift waves in the convection electric field, can trigger substorm expansion phase onset. Recent work by *Rae et al.* [2009a, 2009b] and *Rae et al.* [2010a] also supports this so-called near-geosynchronous onset (NGO) model of substorms. The data presented above also have some features that are consistent with the NGO model. Field-aligned Poynting flux is indeed observed prior to observation of the dipolarization, but subsequent to auroral substorm onset and the detection of the SCW (Figure 8). Drift mode waves are expected to have a component of Poynting flux in the duskward direction and have been previously observed prior to and during expansion phase onset [*Maynard et al.*, 1996a, 1996b]. Duskward Poynting flux was also observed during this event (not shown here). Our observations suggest that the enhanced Poynting flux into the ionosphere expected in the NGO scenario continues after onset as the substorm develops, perhaps powering the aurora, and that TC-2 was not ideally located to measure any enhancements as they first began (or indeed PEACE was still resetting) at expansion phase onset. Also similarly to *Maynard et al.* [1996b], hotter electrons were detected, associated with enhanced earthward convection, a few minutes after the detection of the Poynting flux and substorm onset. Not directly observed by *Maynard et al.* [1996a, 1996b], but observed here, was a low-energy electron population capable of supporting the field-aligned currents associated with the Poynting flux enhancement.

[26] Figures 8c, 8e, and 8f show an enhancement of electron energy flux in both the field-aligned and anti-field-aligned directions for electrons with energies of ~0.1–5 keV. This enhancement lasted ~150 s. The difference between the flux of electrons with a pitch angle of 0° and a pitch angle of 180° (Figure 8g) was close to zero for the majority of this interval, which indicates that for the most part, there was no net electron energy flux in either direction along the field line, even though the average of the flux in the parallel and antiparallel directions is enhanced above the perpendicular flux. Figure 8g shows a temporary imbalance between parallel and antiparallel energy flux between 0423:50 UT and 0424:07 UT. The red color in Figure 8g indicates a net flux of electrons parallel to the magnetic field and hence directed toward the northern ionosphere. This was immediately followed by an enhanced net flux antiparallel to the magnetic field (i.e., out of the northern ionosphere)of similar duration. This short-lived signature of net field-aligned flux into and out of the northern ionosphere appears to be superimposed upon a background of warm (~2 keV) electrons which are evident at all pitch angles. This is presumably the plasma sheet population and shows little modulation throughout this interval (see Figure 8d). The field-aligned and anti-field-aligned flux enhancements are interesting, since they are measured only a few minutes after substorm onset, a period during which electron precipitation and field-aligned currents are important. Below, we discuss some potential explanations for this brief burst of net field-aligned energy flux directed first toward then away from the northern ionosphere. The possibility that the field-aligned electron enhancements seen in Figure 8g are due to pitch angle scattering of plasma sheet electrons into the loss cone appears remote, since this cannot explain the direction change from parallel to antiparallel at 0424:10 UT.

[27] The enhancement in net parallel electron flux occurs at the same time as the burst of field-aligned Poynting flux directed toward the northern ionosphere and is of similar duration. The field-aligned Poynting flux is due to perturbations in the perpendicular electric and magnetic fields. The contemporaneous nature of the enhancements in the net parallel electron energy flux and field-aligned Poynting flux, and their common direction, leads us to investigate the possibility that the field perturbations and the parallel electron enhancements are linked by shear Alfvén waves. The local magnetic field strength is ~100 nT, so the local proton gyrofrequency is Ω_p = 2 Hz. The frequency range of the Poynting flux shown in Figure 8 is 16–68 mHz, significantly

less than Ω_p, consistent with the Poynting flux being provided by shear-mode Alfvén waves. Using the electric field estimates shown in Figure 8, we calculate the ratio of perpendicular field perturbations $E_r/B_\phi \sim 4.5 \times 10^4$ km s^{-1} and $E_\phi/B_r \sim 4.0 \times 10^4$ km s^{-1}. The local Alfvén velocity is $v_A \sim$ 2500 km s^{-1}, given a local number density $n_e \sim 0.75$ cm^{-3} (see Figure 5). The ratio of electric to magnetic field will only yield the phase speed of the wave if the wave is propagating. If these field perturbations represent standing Alfvén waves, then this ratio can take any value, depending upon the spacecraft location relative to the wave nodes. The plasma parameters are such that the local electron thermal speed is 10 times the size of the local Alfvén speed, so any shear Alfvén wave present will be subject to kinetic effects if it possesses small perpendicular scales. If these perpendicular field perturbations are due to shear Alfvén waves, then the enhancement of parallel then antiparallel 100–1000 eV electrons could be the signature of the parallel current perturbation associated with the wave [*Watt et al.*, 2005], although this would imply that the waves have short perpendicular scale lengths. The qualitative association we have made between the net parallel electron enhancement, enhanced ULF wave power, and field-aligned Poynting flux is consistent with the idea that shear mode Alfvén waves can link these phenomena and indeed power the aurora [*Watt and Rankin*, 2009; *Watt and Rankin*, 2010]. More detailed analysis of similar events where more comprehensive data are available, however, is required to establish the quantitative and physical relationship between the net field-aligned electron energy flux and the net field-aligned Poynting flux observed by TC-2.

[28] Note that in the detailed in situ observations of field-aligned low-energy electrons, Poynting flux is only encountered by the TC-2 spacecraft for a short period, whereas the auroral brightening associated with this substorm lasts for ~30 minutes. Owing to the dynamic nature of the magnetotail during this time, the latitudinally confined auroral display, and the transient passage of the TC-2 spacecraft through the region of auroral field lines, we would not expect TC-2 to observe the in situ signature of the auroral acceleration mechanism for the entire duration of the auroral display. Furthermore, the nature of the auroral acceleration mechanism may change during the substorm expansion phase [*Newell et al.*, 2010]. Further investigation of multispacecraft observations is required to determine the evolution of substorm-related precipitation [e.g., *Hull et al.*, 2010].

[29] Recent work by *Nakamura et al.* [2009] employed Cluster data to suggest that rapid flux transport via BBFs and the arrival of transient dipolarization fronts into the 10 R_E region drive the near-tail unstable (as evidenced by fluctuations in the magnetic field), resulting in a tailward propagating, more global dipolarization. This is in contrast to the work of *Maynard et al.* [1996a, 1996b] and *Erickson et al.* [2000]. Although during this event TC-2 and GOES-12 were located earthward of the position of Cluster during the event reported in *Nakamura et al.* [2009], both spacecraft observed a similar magnetic signature in that wave activity was observed prior to a large-scale dipolarization. Contrary to *Nakamura et al.* [2009], however, no earthward flux transport was observed prior to the wave activity, nor was a tailward-propagating global dipolarization. Indeed, the converse was observed: The global dipolarization as detected by TC-2 was accompanied by fast earthward flows, suggesting an earthward propagation from further downtail than TC-2. That the dipolarization was detected at GOES-12 before TC-2, which was located slightly earthward of GOES-12, is also consistent with this. It is possible that any initial earthward flux transport and associated transient dipolarization fronts stopped prior to reaching the geosynchronous region and the global dipolarization propagated both earthward and tailward from that point in a similar manner to energetic particle injection regions [e.g., *Lopez et al.*, 1990].

[30] Data from Cluster, which was located ~15 R_E downtail at a similar local time to TC-2 (not shown), indicate that the spacecraft were located in the PSBL in the 30 minutes around substorm onset, so they were not ideally placed to observe any fast flows prior to or after substorm onset. That said, no remote sensing signatures of reconnection and associated flux transport, for example, Travelling Compression Regions [e.g., *Owen et al.*, 2005; *Walsh et al.*, 2007], were observed. Furthermore, *Walsh et al.* [2009] presented evidence that plasma bubbles, thought to carry magnetic flux earthward, can indeed reach the geosynchronous region, and *Takada et al.* [2006] showed that the inward reach of a BBF depends on the prior state (i.e., degree of stretching of the magnetic field) of the inner magnetosphere. If earthward flux transport were responsible for driving the near-earth tail unstable, causing global dipolarization, it is also possible, therefore, that this flux transport would be observed by TC-2 and other geosynchronous spacecraft prior to global dipolarization. Since this was not the case, and the auroral onset occurred at the equatorward edge of the oval, we suggest that the onset location was close to geosynchronous orbit, though with available data for this event, we cannot say whether reconnection in the midtail was ultimately responsible for driving the onset region unstable. Studies of further events using more comprehensively instrumented spacecraft are needed to better link the geosynchronous response to substorm onset with data taken elsewhere in the magnetosphere and ionosphere and to conclusively determine whether earthward flux transport is responsible for driving the geosynchronous region unstable [*Nakamura et al.*, 2009] or whether it is a consequence of substorm onset that is triggered closer to the Earth [e.g., *Maynard et al.*, 1996a; *Lui et al.*, 2008].

5. Summary and Conclusions

[31] We have presented in situ observations from GOES-12 and Double Star TC-2 from within the substorm current wedge and compare them with ground-based magnetometer data and auroral data from both IMAGE and ground-based sources. Using an extension of the AWESOME [*Milling et al.*, 2008; *Murphy et al.*, 2009a] timing technique termed AWESOME:ST, we linked the onset of ULF pulsations in space with ULF onset on the ground and with global auroral substorm onset. An enhancement of field-aligned Poynting flux similar to those observed by *Maynard et al.* [1996a], for example, was also observed. The Poynting flux enhancement was of large enough magnitude to support visible auroral displays and was detected at the same time as increased field-aligned electron differential energy flux, carried by a low-energy population of electrons that were not present after global dipolarization.

The combined observations of the Poynting flux, electron populations, and magnetic ULF wave activity are all consistent with the hypothesis that shear mode Alfvén waves mediate the M-I coupling during this interval and are capable of powering the aurora [e.g., *Watt and Rankin*, 2009; *Watt and Rankin*, 2010].The observed sequence of events is best explained by a near-Earth initiation of the substorm expansion phase onset, such as the Near-Geosynchronous Onset scenario [*Maynard et al.*, 1996b; *Erickson et al.*, 2000], although because of a lack of coverage of the midtail plasma sheet other mechanisms cannot be ruled out.

[32] **Acknowledgments.** APW, ANF, and CF acknowledge funding from UK STFC grant PP/E/001173/1, and APW also acknowledges the Royal Astronomical Society for partially funding this work. IJR, IRM, and CEJW are funded by the CSA. The authors acknowledge the Double Star and FGM and PEACE instrument teams for provision of the TC-2 data; CARISMA and CANMOS magnetometer data were downloaded from the Canadian Space Science Data Portal (http://www.cssdp.ca). NORSTAR MSP data were provided by the University of Calgary.

[33] Robert Lysak thanks Steven Morley and another reviewer for their assistance in evaluating this paper.

References

Akasofu, S. I. (1964), The development of the auroral substorm, *Planet Space Sci.*, *12*(4), 273–282.

Arnoldy, R. L., J. L. Posch, M. J. Engebretson, H. Fukunishi, and H. J. Singer (1998), Pi1 magnetic pulsations in space and at high latitudes on the ground, *J. Geophys. Res.*, *103*, 23,581–23,592, doi:10.1029/98JA01917.

Baker, D. N., T. I. Pulkkinen, V. Angelopoulos, W. Baumjohann, and R. L. McPherron (1996), Neutral line model of substorms: Past results and present view, *J. Geophys. Res.*, *101*, 12,975–13,010, doi:10.1029/95JA03753.

Belian, R. D., G. R. Gisler, T. Cayton, and R. Christiensen (1992), High-Z energetic particles at geosynchronous orbit during the great solar proton event series of October 1989, *J. Geophys. Res.*, *97*(A11), 16,897–16,906, doi:10.1029/92JA01139.

Bösinger, T., and A. G. Yahnin (1987), Pi1B type magnetic pulsation as a high time resolution monitor of substorm development, *Ann. Geophys.*, *5*, 231–237.

Carr, C., et al. (2005), The Double Star magnetic field investigation: Instrument design, performance and highlights of the first year's observations, *Ann. Geophys.*, *23*, 2713–2732.

Chaston, C. C., et al. (2005), Energy deposition by Alfvén waves into the dayside auroral oval: Cluster and FAST observations, *J. Geophys. Res.*, *110*, A02211, doi:10.1029/2004JA010483.

Donovan, E. F., B. J. Jackel, I. Voronkov, T. Sotirelis, F. Creutzberg, and N. A. Nicholson (2003), Ground-based optical determination of the b2i boundary: A basis for an optical MT-index, *J. Geophys. Res.*, *108*(A3), 1115, doi:10.1029/2001JA009198.

Erickson, G. M., N. C. Maynard, W. J. Burke, G. R. Wilson, and M. A. Heinemann (2000), Electromagnetics of substorm onsets in the near-geosynchronous plasma sheet, *J. Geophys. Res.*, *105*(A11), 25,265–25,290, doi:10.1029/1999JA000424.

Escoubet, C. P., M. Fehringer, and M. Goldstein (2001), The Cluster mission, *Ann. Geophys.*, *19*, 1197–1200.

Fazakerley, A. N., et al. (2005), The Double Star plasma electron and current experiment, *Ann. Geophys.*, *23*, 2733–2756.

Frey, H. U., and S. B. Mende (2006), Substorm onsets as observed by IMAGE-FUV, in *Proceedings of the Eighth International Conference on Substorms*, edited M. T. Syrjäsuo and E. Donovan, pp. 71–75, Univ. of Calgary, Alberta, Canada.

Gibson, W. C., et al. (2000), The IMAGE Observatory, *Space Sci. Rev.*, *91*, 15–50.

Heacock, R. R. (1967), Two subtypes of type pi micropulsations, *J. Geophys. Res.*, *72*(15), 3905–3917, doi:10.1029/JZ072i015p03905.

Horton, W., H. V. Wong, J. W. Van Dam, and C. Crabtree (2001), Stability properties of high-pressure geotail flux tubes, *J. Geophys. Res.*, *106*, 18,803–18,822, doi:10.1029/2000JA000415.

Hull, A. J., M. Wilber, C. C. Chaston, J. W. Bonnell, J. P. McFadden, F. S. Mozer, M. Fillingim, and M. L. Goldstein (2010), Time development of field-aligned currents, potential drops, and plasma associated with an auroral poleward boundary intensification, *J. Geophys. Res.*, *115*, A06211, doi:10.1029/2009JA014651.

Jacobs, J. A., Y. Kato, S. Matsushita, and V. A. Troitskaya (1964), Classification of Geomagnetic Micropulsations, *J. Geophys. Res.*, *69*, 180–181, doi:10.1029/JZ069i001p00180.

Kepko, L., and M. Kivelson (1999), Generation of Pi2 pulsations by bursty bulk flows, *J. Geophys. Res.*, *104*, 25,021–25,034, doi:10.1029/1999JA900361.

Lessard, M. R., E. J. Lund, S. L. Jones, R. L. Arnoldy, J. L. Posch, M. J. Engebretson, and K. Hayashi (2006), Nature of Pi1B pulsations as inferred from ground and satellite observations, *Geophys. Res. Lett.*, *33*, L14108, doi:10.1029/2006GL026411.

Liu, Z. X., C. P. Escoubet, Z. Pu, H. Laakso, J. K. Shi, C. Shen, and M. Hapgood (2005), The Double Star mission, *Ann. Geophys.*, *23*, 2707–2712.

Lopez, R. E., D. G. Sibeck, R. W. McEntire, and S. M. Krimigis (1990), The energetic ion substorm injection boundary, *J. Geophys. Res.*, *95*, 109–117, doi:10.1029/JA095iA01p00109.

Lui, A. T. Y. (1996), Current disruption in the Earth's magnetosphere: Observations and models, *J. Geophys. Res.*, *101*, 13,067–13,088, doi:10.1029/96JA00079.

Lui, A. T. Y. (2004), Potential plasma instabilities for substorm expansion onsets, *Space Sci. Rev.*, *113*, 127–206, doi:10.1023/B:SPAC.0000042942.00362.4e.

Lui, A. T. Y., et al. (2008), Near-Earth substorm features from multiple satellite observations, *J. Geophys. Res.*, *113*, A07S26, doi:10.1029/2007JA012738.

Mann, I. R., et al. (2008), The upgraded CARISMA magnetometer array in the THEMIS era, *Space Sci. Rev.*, *141*(1–4), 413–451, doi:10.1007/s11214-008-9457-6.

Maynard, N. C., W. J. Burke, E. M. Basinska, G. M. Erickson, W. J. Hughes, H. J. Singer, A. G. Yahnin, D. A. Hardy, and F. S. Mozer (1996a), Dynamics of the inner magnetosphere near times of substorm onsets, *J. Geophys. Res.*, *101*, 7705–7736, doi:10.1029/95JA03856.

Maynard, N. C., W. J. Burke, G. M. Erickson, E. M. Basinska, and A. G. Yahnin (1996b), Magnetosphere-ionosphere coupling during substorm onset, in *International Conference on Substorms, ESA Special Publication*, vol. 389, edited by E. J. Rolfe and B. Kaldeich, pp. 301–305, Eur. Space Agency, Paris.

McPherron, R. L., C. T. Russell, and M. P. Aubry (1973), Satellite studies of magnetospheric substorms on August 15, 1968. 9. Phenomenological model for substorms, *J. Geophys. Res.*, *78*, 3131–3149, doi:10.1029/JA078i016p03131.

Mende, S. B., et al. (2000a), Far ultraviolet imaging from the IMAGE spacecraft. 1. System design, *Space Sci. Rev.*, *91*(1–2), 243–270.

Mende, S. B., et al. (2000b), Far ultraviolet imaging from the IMAGE spacecraft. 2. Wideband FUV imaging, *Space Sci. Rev.*, *91*(1–2), 271–285.

Milan, S. E., A. Grocott, and B. Hubert (2010), A superposed epoch analysis of auroral evolution during substorms: Local time of onset region, *J. Geophys. Res.*, *115*, A00I04, doi:10.1029/2010JA015663.

Milling, D. K., I. J. Rae, I. R. Mann, K. R. Murphy, A. Kale, C. T. Russell, V. Angelopoulos, and S. Mende (2008), Ionospheric localisation and expansion of long-period Pi1 pulsations at substorm onset, *Geophys. Res. Lett.*, *35*, L17S20, doi:10.1029/2008GL033672.

Murphy, K. R., I. J. Rae, I. R. Mann, D. K. Milling, C. E. J. Watt, L. Ozeke, H. U. Frey, V. Angelopoulos, and C. T. Russell (2009a), Wavelet-based ULF wave diagnosis of substorm expansion phase onset, *J. Geophys. Res.*, *114*, A00C16, doi:10.1029/2008JA013548.

Murphy, K. R., et al. (2009b), Reply to comment by K. Liou and Y.-L. Zhang on "Wavelet-based ULF wave diagnosis of substorm expansion phase onset", *J. Geophys. Res.*, *114*, A10207, doi:10.1029/2009JA014351.

Murphy, K. R., I. J. Rae, I. R. Mann, and D. K. Milling (2010), On the nature of ULF wave power during nightside auroral activations and substorms: 1. Spatial distribution, *J. Geophys. Res.*, doi:10.1029/2010JA015757, in press.

Nagai, T., R. Nakamura, T. Mukai, T. Yamamoto, A. Nishida, and S. Kokubun (1997), Substorms, tail flows and plasmoids, *Adv. Space Res.*, *20*, 961–971, doi:10.1016/S0273-1177(97)00504-8.

Nakamura, R., et al. (2009), Evolution of dipolarization in the near-Earth current sheet induced by Earthward rapid flux transport, *Ann. Geophys.*, *27*, 1743–1754.

Newell, P. T., A. R. Lee, K. Liou, S. Ohtani, T. Sotirelis, and S. Wing (2010), Substorm cycle dependence of various types of aurora, *J. Geophys. Res.*, *115*, A09226, doi:10.1029/2010JA015331.

Ohtani, S.-I. (2004), Flow bursts in the plasma sheet and auroral substorm onset: Observational constraints on connection between midtail and near-Earth substorm processes, *Space Sci. Rev.*, *113*, 77–96, doi:10.1023/B:SPAC.0000042940.59358.2f.

Olson, J. V. (1999), Pi2 pulsations and substorm onsets: A review, *J. Geophys. Res.*, *104*, 17,499–17,520, doi:10.1029/1999JA900086.

Østgaard, N., S. B. Mende, H. U. Frey, T. J. Immel, L. A. Frank, J. B. Sigwarth, and T. J. Stubbs (2004), Interplanetary magnetic field control of the location of substorm onset and auroral features in the conjugate hemispheres, *J. Geophys. Res.*, *109*, A07204, doi:10.1029/2003JA010370.

Owen, C. J., J. A. Slavin, A. N. Fazakerley, M. W. Dunlop, and A. Balogh (2005), Cluster electron observations of the separatrix layer during traveling compression regions, *Geophys. Res. Lett.*, *32*, L03104, doi:10.1029/2004GL021767.

Rae, I. J., et al. (2009a), Timing and localization of ionospheric signatures associated with substorm expansion phase onset, *J. Geophys. Res.*, *114*, A00C09, doi:10.1029/2008JA013559.

Rae, I. J., et al. (2009b), Near-Earth initiation of a terrestrial substorm, *J. Geophys. Res.*, *114*, A07220, doi:10.1029/2008JA013771.

Rae, I. J., C. E. J. Watt, I. R. Mann, J. C. Samson, K. Kabin, and V. Angelopoulos (2010a), Optical characterization of the growth and spatial structure of a substorm onset arc, *J. Geophys. Res.*, *115*, A10222, doi:10.1029/2010JA015376.

Rae, I. J., K. R. Murphy, C. E. J. Watt, and I. R. Mann (2010b), On the nature of ULF wave power during nightside auroral activations and substorms: 2. Temporal evolution, *J. Geophys. Res.*, doi:10.1029/2010JA015762, in press.

Rostoker, G., J. C. Samson, F. Creutzberg, T. J. Hughes, D. R. McDiarmid, A. G. McNamara, A. V. Jones, D. D. Wallis, and L. L. Cogger (1995), Canopus: A ground-based instrument array for remote sensing the high latitude ionosphere during the ISTP/GGS program, *Space Sci. Rev.*, *71*, 743–760, doi:10.1007/BF00751349.

Saito, M. H., Y. Miyashita, M. Fujimoto, I. Shinohara, Y. Saito, K. Liou, and T. Mukai (2008), Ballooning mode waves prior to substorm-associated dipolarizations: Geotail observations, *Geophys. Res. Lett.*, *35*, L07103, doi:10.1029/2008GL033269.

Shiokawa, K., W. Baumjohann, and G. Haerendel (1997), Braking of high-speed flows in the near-Earth tail, *Geophys. Res. Lett.*, *24*, 1179–1182, doi:10.1029/97GL01062.

Sibeck, D. G., and V. Angelopoulos (2008), THEMIS science objectives and mission phases, *Space Sci. Rev.*, *141*, 35–59, doi:10.1007/s11214-008-9393-5.

Singer, H., L. Matheson, R. Grubb, A. Newman, and D. Bouwer (1996), Monitoring space weather with the GOES magnetometers, in *Society of Photo-Optical Instrumentation Engineers (SPIE) Conference Series*, vol. 2812, edited by E. R. Washwell, pp. 299–308.

Smith, A. J., M. P. Freeman, S. Hunter, and D. K. Milling (2002), VLF, magnetic bay, and Pi2 substorm signatures at auroral and midlatitude ground stations, *J. Geophys. Res.*, *107*(A12), 1439, doi:10.1029/2002JA009389.

Spanswick, E., E. Donovan, R. Friedel, and A. Korth (2007), Ground based identification of dispersionless electron injections, *Geophys. Res. Lett.*, *34*, L03101, doi:10.1029/2006GL028329.

Stenbaek-Nielsen, H. C., T. J. Hallinan, D. L. Osborne, J. Kimball, C. Chaston, J. McFadden, G. Delory, M. Temerin, and C. W. Carlson (1998), Aircraft observations conjugate to FAST: Auroral arc thicknesses, *Geophys. Res. Lett.*, *25*, 2073–2076, doi:10.1029/98GL01058.

Stewart, B. (1861), On the great magnetic disturbance which extended from august 28 to september 7, 1859, as recorded by photography at the kew observatory, *Phil. Trans. R. Soc. London*, *151*, 423–430.

Takada, T., et al. (2006), Do BBFs contribute to inner magnetosphere dipolarizations: Concurrent Cluster and Double Star observations, *Geophys. Res. Lett.*, *33*, L21109, doi:10.1029/2006GL027440.

Tsyganenko, N. A., and D. P. Stern (1996), Modeling the global magnetic field of the large-scale Birkeland current systems, *J. Geophys. Res.*, *101*, 27,187–27,198, doi:10.1029/96JA02735.

Volwerk, M., et al. (2005), Plasma flow channels with ulf waves observed by cluster and double star, *Ann. Geophys.*, *23*(8), 2929–2935.

Voronkov, I., R. Rankin, P. Frycz, V. T. Tikhonchuk, and J. C. Samson (1997), Coupling of shear flow and pressure gradient instabilities, *J. Geophys. Res.*, *102*, 9639–9650, doi:10.1029/97JA00386.

Walsh, A. P., A. N. Fazakerley, R. J. Wilson, I. V. Alexeev, P. D. Henderson, C. J. Owen, E. Lucek, C. Carr, and I. Dandouras (2007), Near-simultaneous magnetotail flux rope observations with Cluster and Double Star, *Ann. Geophys.*, *25*, 1887–1897.

Walsh, A. P., et al. (2009), Cluster and Double Star multipoint observations of a plasma bubble, *Ann. Geophys.*, *27*, 725–743.

Watt, C. E. J., and R. Rankin (2009), Electron trapping in shear Alfvén waves that power the aurora, *Phys. Rev. Lett.*, *102*(4), 045002, doi:10.1103/PhysRevLett.102.045002.

Watt, C. E. J., and R. Rankin (2010), Do magnetospheric shear Alfvén wave generate sufficient electron energy flux to power the aurora?, *J. Geophys. Res.*, *115*, A07224, doi:10.1029/2009JA015185.

Watt, C. E. J., R. Rankin, I. J. Rae, and D. M. Wright (2005), Self-consistent electron acceleration due to inertial Alfvén wave pulses, *J. Geophys. Res.*, *110*, A10S07, doi:10.1029/2004JA010877.

Wygant, J. R., et al. (2002), Evidence for kinetic Alfvén waves and parallel electron energization at 4–6 R_E altitudes in the plasma sheet boundary layer, *J. Geophys. Res.*, *107*(A8), 1201, doi:10.1029/2001JA900113.

Yumoto, K., and The CPMN Group (2001), Characteristics of Pi 2 magnetic pulsations observed at the CPMN stations: A review of the STEP results, *Earth Planets Space*, *53*, 981–992.

E. F. Donovan, Department of Physics and Astronomy, University of Calgary, Calgary, Alberta, Canada.

A. N. Fazakerley, C. Forsyth, and A. P. Walsh, Mullard Space Science Laboratory, University College London, Holmbury St. Mary, Dorking, Surrey, RH5 6NT, UK. (apw@mssl.ucl.ac.uk)

I. R. Mann, K. R. Murphy, I. J. Rae, and C. E. J. Watt, Department of Physics, University of Alberta, Edmonton, Alberta, Canada.

H. J. Singer, NOAA, Space Weather Prediction Center, Boulder, CO, USA.

M. Volwerk and T. L. Zhang, Space Research Institute, Austrian Academy of Sciences, Graz, Austria.